Delft University of Technology

High-temperature nanoindentation characterization of sintered nano-copper particles used in high power electronics packaging

Fan, Jiajie; Jiang, Dawei; Zhang, Hao; Hu, Dong; Liu, Xu; Fan, Xuejun; Zhang, Guoqi

DOI
10.1016/j.rinp.2021.105168

Publication date
2022

Document Version
Final published version

Published in
Results in Physics

Citation (APA)
Fan, J., Jiang, D., Zhang, H., Hu, D., Liu, X., Fan, X., & Zhang, G. (2022). High-temperature nanoindentation characterization of sintered nano-copper particles used in high power electronics packaging. *Results in Physics*, *33*, Article 105168. https://doi.org/10.1016/j.rinp.2021.105168

Important note
To cite this publication, please use the final published version (if applicable).
Please check the document version above.

Copyright
Other than for strictly personal use, it is not permitted to download, forward or distribute the text or part of it, without the consent of the author(s) and/or copyright holder(s), unless the work is under an open content license such as Creative Commons.

Takedown policy
Please contact us and provide details if you believe this document breaches copyrights.
We will remove access to the work immediately and investigate your claim.

This work is downloaded from Delft University of Technology.
For technical reasons the number of authors shown on this cover page is limited to a maximum of 10.

Results in Physics 33 (2022) 105168

Contents lists available at ScienceDirect

Results in Physics

journal homepage: www.elsevier.com/locate/rinp

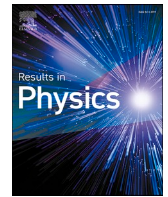

High-temperature nanoindentation characterization of sintered nano-copper particles used in high power electronics packaging

Jiajie Fan [a,b,*], Dawei Jiang [c], Hao Zhang [d], Dong Hu [e], Xu Liu [e], Xuejun Fan [f], Guoqi Zhang [e]

[a] Institute of Future Lighting, Academy for Engineering & Technology, Fudan University, Shanghai 200433, China
[b] Shanghai Engineering Technology Research Center for SiC Power Device, Fudan University, Shanghai 200433, China
[c] College of Mechanical and Electrical Engineering, Hohai University, Changzhou 213022, China
[d] School of Materials Science and Engineering, Nanyang Technological University, Singapore 639798, Singapore
[e] Department of Microelectronics Engineering, Delft University of Technology, 2628 Delft, The Netherlands
[f] Department of Mechanical Engineering, Lamar University, Beaumont, TX 77705, USA

A R T I C L E I N F O

Keywords:
Power electronics packaging
Nano-copper sintering
Nanoindentation
High-temperature creep
Reliability

A B S T R A C T

Nano-copper sintering is one of new die-attachment and interconnection solutions to realize the wide bandgap semiconductor power electronics packaging with benefits on high temperature, low inductance, low thermal resistance and low cost. Aiming to assess the high-temperature reliability of sintered nano-copper die-attachment and interconnection, this study characterized the mechanical properties of sintered nano-copper particles using the high-temperature nanoindentation tests. The results showed that: firstly, the hardness and indentation modulus of the sintered nano-copper particles increased rapidly when the loading rate increased below 0.2 $mN{\cdot}s^{-1}$ and then stabilized, and decreased with increased applied load up to 30 mN. Next, by extracting the yield stress and strain hardening index, a plastic stress–strain constitutive model at room temperature for sintered nano-copper particles was obtained. Finally, the high temperature nanoindentation tests were performed at 140 ℃–200 ℃ on the sintered nano-copper particles prepared under different assisted pressures, which showed that a high assisted pressure resulted in the reduced temperature sensitivity of hardness and indentation modulus. The creep tests indicated that high operation temperature resulted in a high steady-state creep rate, which negatively impacted the creep resistance of sintered nano-copper particles, while the higher assisted pressure could improve the creep resistance.

Introduction

The wide bandgap (WBG) semiconductors, represented by SiC and GaN, have become great candidates in high power electronics due to their advantages of higher power density, breakdown voltage, and operation temperature compared to Si. Due to the European Union's restriction on lead electronics, the die-attachment and interconnection materials used in high power electronics packaging require the lead-free alternatives. One of representative lead-free materials is Sn-Ag-Cu (SAC) solder, which has replaced the widely used SnPb solder in the most of electronics industry [1]. However, the SAC solder always suffers several limitations on high temperature operation, corrosion resistances, tin-whisker caused by migration and fatigue fracture caused by brittle intermetallic compounds, and so on. Based on the size effect of nano-materials, nano-metal particle sintering technology realizes the functions of low-temperature packaging and high-temperature service for high power electronics [2]. Compared with nano-silver that already widely used in industry, nano-copper has a higher melting point, lower material cost, excellent thermal conductivity, and matching thermal expansion coefficient, and it is expected to become one of the main die-attachment and interconnection technologies in the future high power electronics packaging with "all-copper packaging" as a technical possibility[3,4].

The high temperature mechanical performances of sintered nano-copper materials are essential to guarantee the package and module level reliability of power electronics, as they will suffer thermal fatigue and creep failures when exposed to high temperature cycling application conditions [5]. Thus, it is necessary to investigate the mechanical deformation behavior of sintered nano-copper materials at high temperatures and establish the reasonable constitutive models used in

* Corresponding author at: Institute of Future Lighting, Academy for Engineering & Technology, Fudan University, Shanghai 200433, China.
E-mail address: jiajie_fan@fudan.edu.cn (J. Fan).

https://doi.org/10.1016/j.rinp.2021.105168
Received 17 September 2021; Received in revised form 25 December 2021; Accepted 27 December 2021
Available online 28 December 2021
2211-3797/© 2021 The Author(s). Published by Elsevier B.V. This is an open access article under the CC BY-NC-ND license (http://creativecommons.org/licenses/by-nc-nd/4.0/).

reliability and lifetime estimation [6,7]. Presently, a common method to characterize the mechanical properties of sintered nano-metal materials is through the stress–strain relationship obtained by uniaxial tensile or shear tests [8–12]. For example, Nishikawa *et al.* [13] studied the influence of sintering process parameters on the connection performance of copper–copper interconnection joints and found that the preheating and sintering temperatures and the protective atmosphere significantly affected the shear performance of the joints. A copper–copper interconnection joint with a high shear strength about 40 MPa was successfully obtained at a sintering temperature of 400 C and pressure of 15 MPa. Yamakawa *et al.* [14] also investigated the effects of sintering pressure on the shear strength of the sintered nano-copper joint and obtained a joint with a shear strength about 30 MPa at a temperature of 250℃ and a pressure of 15 MPa. Furthermore, Zuo *et al.* [15] prepared a copper paste using a proportionate mixture of 20 and 100 nm copper nanoparticles, and the strength of the prepared sample was 15 MPa at a sintering temperature of 250℃ and sintering pressure of 4 MPa. However, compared with traditional solder materials, the preparation of large standard tensile test samples through sintering is difficult, as the assist-pressure and sample shrinkage and warpage are difficult to be controlled during sintering [16–18]. The nanoindentation test can realize a multi-point test on a small area under elevated temperature conditions, making it as a more convenient method to characterize the high temperature mechanical properties, obtain a constitutive relationship model and assess scale-dependent creep properties for the sintered materials [19].

Aiming to assess the high temperature reliability of sintered nano-copper particles used in high power electronics packaging, the nanoindentation technique was applied in this study to characterize their high temperature mechanical properties, i.e. indentation hardness, indentation modulus, and creep properties. The remaining part of this paper is organized as follows: Section 2 introduces the methods of sample preparation and test process. In section 3, the effects of strain rate and applied load on the indentation hardness of sintered nano-copper particles were firstly analyzed. Then, a stress–strain constitutive model for nano-copper sintered materials at room temperature was constructed to assess their elastic–plastic behaviors. Next, the effects of temperature and assisted pressure on indentation depth, hardness, and indentation modulus were studied, and the effects of temperature and assisted pressure on the initial creep behavior of nano-copper sintered particles were analyzed. Finally, section 4 presents the concluding remarks.

Sample preparation and nanoindentation test

Test sample preparation

In order to prevent the oxidation of raw materials, the test sample preparation was conducted in a nitrogen glove box. To guarantee the better sintering densification, the sample preparation process refers to our previous work [20] as shown in Fig. 1 (a-b). Firstly, 250 nm and 50 nm nano-copper powders were mixed at a mass ratio of 8:1 with ethanol, 1.5 g of the mixed nano-copper powders were then placed in a mold and several pressures of 10, 20, and 30 MPa were applied. Afterward, the pressed mixed powders were placed in a vacuum sintering furnace and heated up to 300 C at a heating rate of 5 C/min, and after 40 min of sintering, it was naturally cooled to room temperature. Finally, the surfaces of sintered samples were polished to be used for the next nanoindentation test as shown in Fig. 1 (c).

Nanoindentation test

Fig. 2 (a) describes a typical load–displacement curve in a nanoindentation test, and the indenter parameters after indentation and unloading are shown in Fig. 2 (b). As shows, F_{max} and h_{max} are the peak load and the corresponding maximum indentation depth, respectively; h_p is the residual depth after unloading; and S is the contact stiffness, which is the slope at the top of the unloading curve. The displacement of the intersection of the tangent and the coordinate axis is defined by h_r.

The projected area A_c of the contact surface of the Berkovich indenter, and the contact depth h_c between the indenter and test sample were calculated using the following equations [21]:

$$A_c = 24.56h_c^2 \quad (1)$$

$$h_c = h_{max} - \varepsilon(h_{max} - h_r) \quad (2)$$

where ε is the indenter shape correction coefficient that depends on the geometry of the indenter. Here, $\varepsilon = 0.75$ for a triangular pyramid indenter. h_r is the intersection of the tangent line at the maximum load and the displacement axis during unloading.

Hardness is the resistance to local deformation and is an important mechanical parameter to be measured in the nanoindentation test, as well as an important criteria to evaluate the mechanical properties of materials. Hardness is contributed by the average stress of an indenter acting on the surface of a material. During the indentation process, a large number of various dislocations will occur near the indenter, and the hardness value will usually decrease as the load increases. However, the hardness value of some nanomaterials does not change with a change in load [22]. According to Equation (3), the hardness H can be defined as the maximum indentation load F_{max} divided by the projected contact area of the indenter A_c [23]:

$$H = \frac{F_{max}}{A_c} \quad (3)$$

Creep is one of time-dependent mechanical properties of metal materials, which refers to the slow, continuous, and unrecoverable deformation under constant temperature, load, and long-term action. Essentially, it is the process of elastic strain in metals that gradually transforms into inelastic strain over time. As shown in Fig. 3, a typical creep displacement curve, under certain temperatures and loads, creep can be roughly divided into three stages over time: (i) Initial creep; (ii) Steady creep; and (iii) Accelerated creep. For the indentation test, a constant load is applied to the indenter, the load is kept at maximum load for a certain period of time, and the relationship curve between the

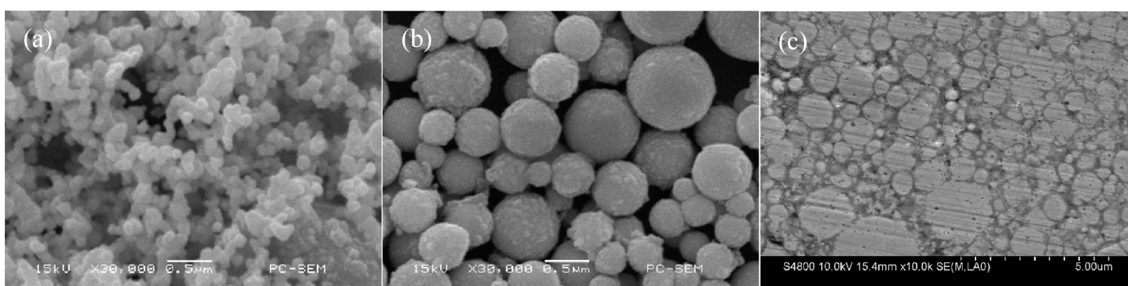

Fig. 1. (a) 50 nm nano-copper particles; (b) 250 nm nano-copper particles; (c) the surface of sintered sample used for nanoindentation test.

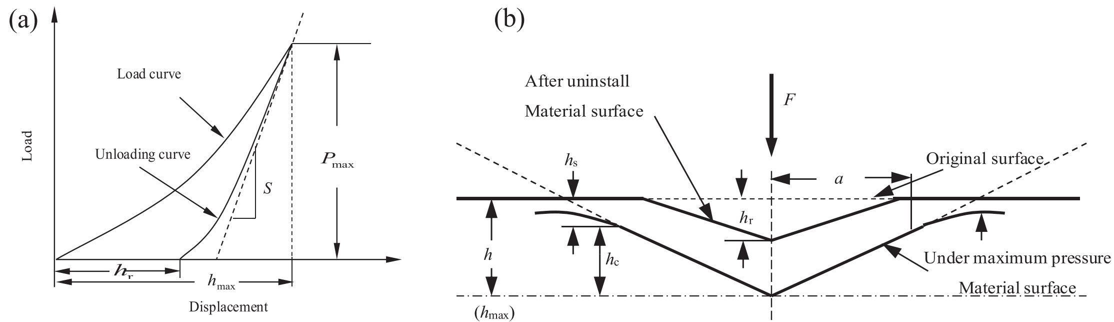

Fig. 2. (a) Typical load–displacement curve in a nanoindentation test; (b) Schematic of the indenter parameters.

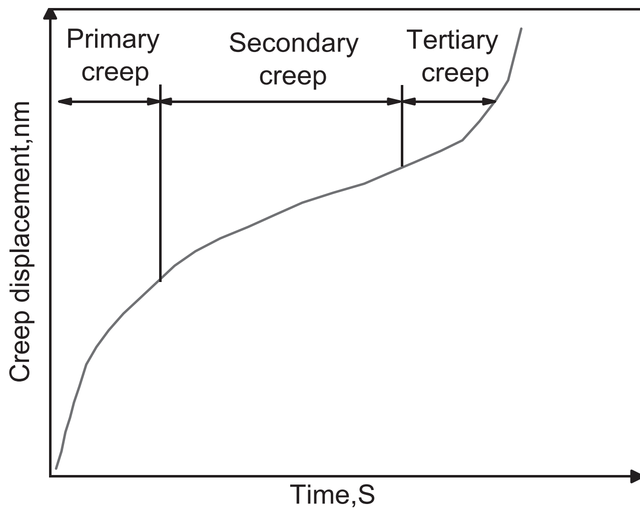

Fig. 3. Typical creep displacement curve.

indenter displacement and time is recorded. During the initial creep stage, the creep displacement increases rapidly, and as creep time is extended, creep displacement increases gradually and slows down as it enters the steady creep stage. At this point, creep time and displacement are approximately linear. The second stage in the creep process, or the steady creep stage, has the smallest creep rate and is often used to measure the creep deformation resistance of materials. Therefore, it is important to investigate the change law of steady-state creep stage and construct a steady-state creep constitutive model by using a constitutive equation.

In the steady creep stage of nanoindentation test, the creep rate ($\dot{h}$) and creep strain rate ($\dot{\varepsilon}$) of the material can be expressed by Equations (4) and (5), respectively [24]:

$$\dot{h} = \frac{dh}{dt} \tag{4}$$

$$\dot{\varepsilon} = \frac{1}{h}\frac{dh}{dt} \tag{5}$$

In this study, the nanoindentation tests were conducted under the NanoTest Vantage testing system with a high temperature control platform and the Berkovich diamond indenter (Micro Materials Ltd, Fig. 4 a). The resolution of testing system is 0.1 nm, the load resolution is 30 nN, the temperature control range is from room temperature to 500 ℃, and the temperature control accuracy is ± 0.1 ℃.

The experiment is designed as follows: Firstly, the effects of loading rate on the nanoindentation performance were performed at room temperature, and the peak load was set as 30 mN, the loading rates were 0.1, 0.15, 0.20, 0.25, 0.35, and 0.5 mN·s^{-1}, and the holding time was controlled at 10 s. Next, the influence of the applied load on nanoindentation performance was analyzed with the indentation rate as 0.5 mN·s^{-1} and the maximum loads as 10, 20, 30, 40, and 50 mN. Finally, the temperature effect on nanoindentation performance was studied with the test temperatures controlled as 140, 160, 180, and 200 ℃. These temperature selection was based on the basic temperature requirements for creep: $T/T_m > 0.3$, where T is the test temperature and T_m is the melting point of the material. The melting point T_m of copper is 1083.4 ℃, and the calculated T/T_m values each test temperature were 0.30, 0.32, 0.33, and 0.35, respectively. Therefore, thess selected test temperatures ensured the occurrence of creep and the effectiveness of the test. The load and indentation rates of the variable high temperature test were set to 30 mN and 0.5 mN·s^{-1}, respectively, and the holding time was 300 s.

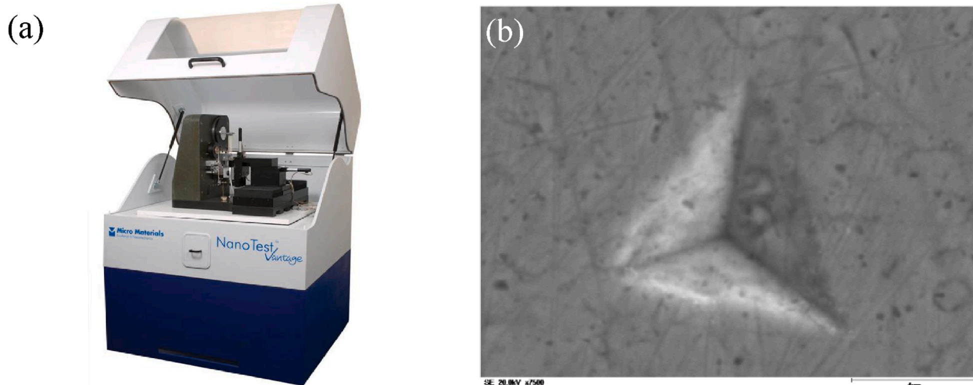

Fig. 4. (a) NanoTest Vantage testing system (cited from www.micromaterials.co.uk); (b) The indentation test points on the sample.

In addition, to avoid the effects of adjacent indentation stress fields, the distance between adjacent indentations was three times greater than the indentation size, and 10 different positions were measured under the same experimental parameters. The indentation morphologies of test samples were then observed and analyzed by Scanning Electron Microscope (SEM) as shown in Fig. 4 b.

Results and discussion

Room-temperature nanoindentation test result analysis

The effect of loading rate on indentation performance

Fig. 5 (a) shows the load–displacement curves of sintered nano-copper particles under different loading rates when the peak load was 30 mN. During loading, the test sample under the indenter experienced the elastic–plastic deformation, and elastic recovery occurred during unloading. As shows, under the same loading conditions, the applied load was sensitive to the loading rate. As the loading rate increased, a larger load was required to reach the same indentation depth, thus, under the same load condition, the greater the loading rate, the smaller the indentation depth, and the steeper the load–displacement curve. Fig. 5 (b) shows the change in indentation performance of test samples with loading rate, which indicates that the hardness and indentation modulus were related to the loading rate. As the loading rate increased, the hardness first increased till 0.2 mN·s^{-1}, and then gradually became stable. This was due to the indentation size and accumulation degree at a low loading rate, which both were greater at higher loading rates and resulted in an increased indentation contact area. According to Equation (3), the indentation hardness obtained at a low strain rate was smaller under the same load. In addition, the strain rate hardening effect leads to higher hardness values obtained at high strain rates. In order to obtain a complete mechanical response, the indentation loading rate of the subsequent experiment was set as 0.5 mN·s^{-1}.

During the indentation process of low-strain hardening materials, a large number of dislocations are produced under the indenter, and the materials under the indenter are plastically deformed due to the movement of dislocations. Because of the movement of indenter, part of the material volume can be pushed to the side of the indenter, and a stacking phenomenon forms. Thus, the stacking phenomenon makes the projected contact area larger than the cross-sectional area of indenter [25]. Fig. 6 shows the indentation morphology images under different loading rates. As the loading rate increased, the indentation size gradually decreased and the degree of stacking around the indentation became continuously smaller. Under the low-loading rate condition, the stress under indenter had more time to release by plastic deformation, thus the indentation size was larger. Furthermore, in order to resist plastic deformation, the material under indenter exhibited more accumulations on the indentation surface and released more stress.

The effect of applied load on indentation performance

When the applied load is large, it takes more time to reach the preset maximum load at the same loading rate, and more plastic deformation occurs under the indenter, which releases the local stress and the indentation size becomes larger. Under a loading rate of 0.5 mN·s^{-1}, the load–displacement curves of the sintered nano-copper particles with different applied loads are shown in Fig. 7 (a). As shows, the indentation depth increased with an increase in applied load. Fig. 7 (b) shows the evolution of hardness and indentation modulus under different loads. As the applied load increased, the hardness values of test samples continuously decreased and gradually stabilized after 30 mN, which exhibited obvious hardness indentation size effects similar to other metal materials. Considering both the effects of loading rate and applied load, a loading rate of 0.5 mN·s^{-1} and a load of 30 mN were selected as the testing parameters for the subsequent elevated temperature experiments.

Plastic stress–strain constitutive modeling

As the metal deformation always consists of elastic strain and plastic strain during the nanoindentation test, the stress–strain relationship of a power strengthening model commonly used in metal materials can be expressed as follows [26]:

$$\sigma = \begin{cases} E\varepsilon(\sigma \leqslant \sigma_y) \\ R\varepsilon^n(\sigma > \sigma_y) \end{cases} \tag{6}$$

where, E is the indentation modulus of the test sample, R is the strength coefficient, and n is the strain hardening index, which reflects a metal's ability to resist uniform plastic deformation. For most metallic materials, the value of n is between 0 and 0.5. Additionally, σ_y is the initial yield stress, and when $\sigma = \sigma_y$, it can be expressed by:

$$\sigma_y = E\varepsilon_y = R\varepsilon_y \tag{7}$$

where, ε_y is the yield strain corresponding to the initial yield stress. Therefore, when the material undergoes elastic and plastic deformation, the total strain is calculated according to:

$$\varepsilon = \varepsilon_y + \varepsilon_p \tag{8}$$

where, ε_p is actual generated plastic strain. According to Equations (7) and (8), when $\sigma > \sigma_y$, the Equation (6) can be changed to:

$$\sigma = \sigma_y\left(1 + \frac{E}{\sigma_y}\varepsilon_p\right)^n \tag{9}$$

After that, the material undergoes elastic–plastic deformation, and

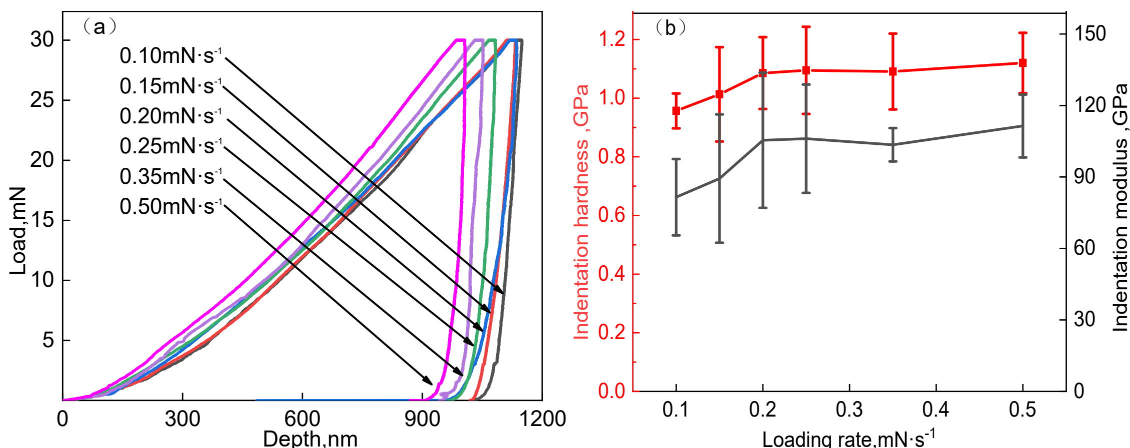

Fig. 5. The effect of loading rate on the indentation properties of sintered nano-copper particles: (a) load–displacement curve; (b) indentation hardness and modulus.

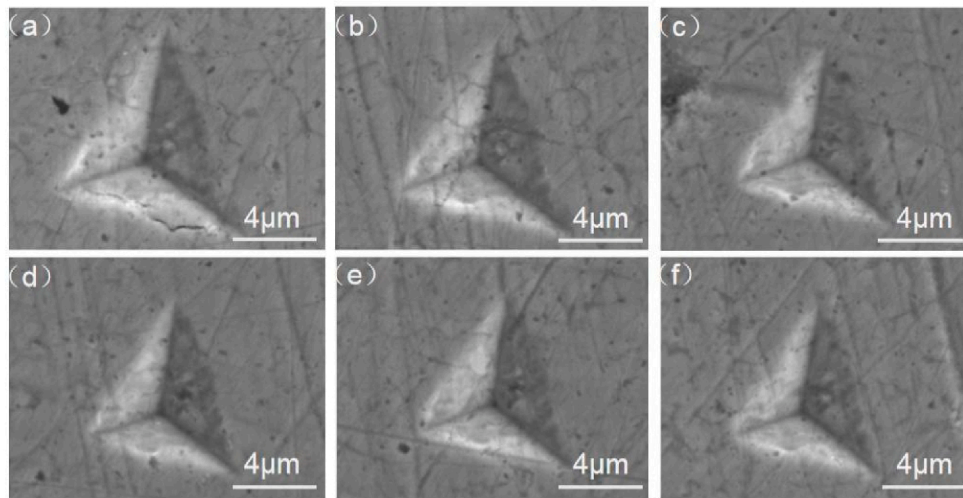

Fig. 6. The indentation morphologies at different loading rates: (a) 0.10 mN·s^{-1}, (b) 0.15 mN·s^{-1}, (c) 0.20 mN·s^{-1}, (d) 0.25 mN·s^{-1}, (e) 0.35 mN·s^{-1}, and (f) 0.50 mN·s^{-1}.

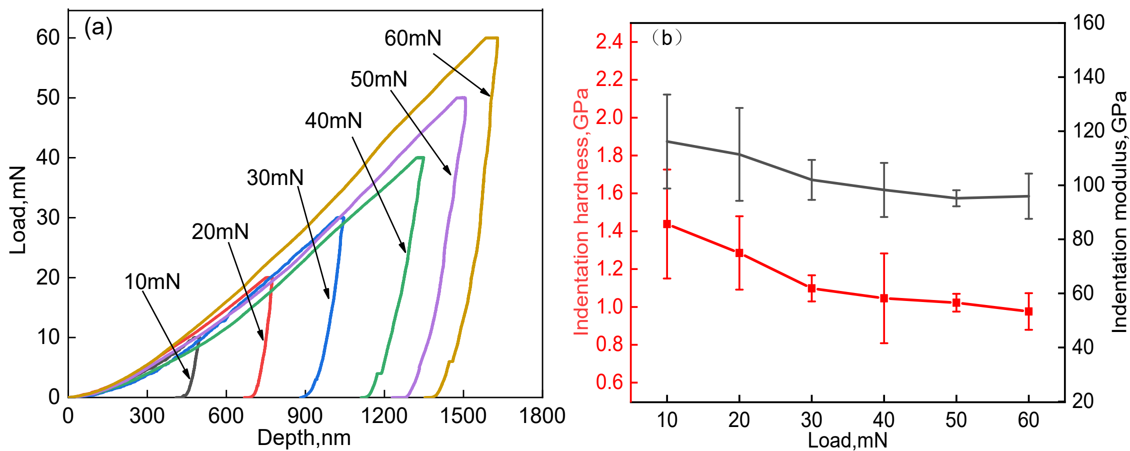

Fig. 7. The effect of applied load on the indentation properties of sintered nano-copper particles: (a) load–displacement curve; (b) indentation hardness and modulus.

the stress–strain relationship is defined by:

$$\sigma = \begin{cases} E\varepsilon(\sigma \leqslant \sigma_y) \\ \sigma_y\left(1 + \frac{E}{\sigma_y}\varepsilon_p\right)^n(\sigma > \sigma_y) \end{cases} \tag{10}$$

With the help of the Oliver–Pharr method [27], the unloading portion of the indentation load–displacement data can be fitted by using the function of Equation (6), which is defined by:

$$F = B(h - h_p)^m \tag{11}$$

where, B and m are the fitting parameters for the initial stage of the unloading curve using the least square method, and the fitting range is generally selected from the initial unloading point to 25%–50% of the upper portion of the unloading curve. The contact stiffness S can also be calculated by the differential Equation (11):

$$S = \left.\frac{\mathrm{d}F}{\mathrm{d}h}\right|_{h=h_{\max}} = mB(h_{max} - h_p)^{m-1} \tag{12}$$

The equivalent indentation modulus E_r is expressed as:

$$\frac{1}{E_r} = \frac{1 - \nu^2}{E} + \frac{1 - \nu_i^2}{E_i} \tag{13}$$

where, E_i and ν_i are the indentation modulus (1140 GPa) and Poisson's ratio (0.07) of the indenter, respectively, and E and ν are the indentation modulus and Poisson's ratio (0.3) of the test samples, respectively. The equivalent indentation modulus can be obtained from the unloading curve as follows:

$$S = \left.\frac{dF}{dh}\right|_{h=h_{max}} = \frac{2}{\sqrt{\pi}}E_r\sqrt{A_c} \tag{14}$$

and therefore

$$E_r = \frac{\sqrt{\pi}}{2}\cdot\frac{S}{\sqrt{A_c}} \tag{15}$$

Thus, after the hardness H of a material is determined, the yield stress σ_y can be evaluated according to the hardness [28]. For the Berkovich diamond indenter whose equivalent half cone angle is $\alpha = 70.3^\circ$, the flow stress yield criterion one (von Mises yield criterion one) is used to predict the yield stress σ_y. For many metals, the approximate relationship between the yield stress and the hardness is given by [29]:

$$\sigma_y \approx \frac{H}{3} \tag{16}$$

Moreover, Giannakopoulos and Sureshl [30] used finite element

analysis to assess the indentation test of a Berkovich indenter and obtained a plastic representative strain of 29%. In the subsequent discussion, the plastic characteristic strain value was 0.29.

The ratio of residual depth indentation h_p to the corresponding maximum depth h_{max} at unloading can be used to express the degree of plastic deformation and strain hardening of the material, as shown in Equation (17) [30]:

$$\frac{\sigma_{0.29}-\sigma_y}{0.29E_r}=1-0.142\frac{h_p}{h_{max}}-0.957\left(\frac{h_p}{h_{max}}\right)^2 \quad (17)$$

Thus, the strain hardening index of materials can be obtained by determining the loading and unloading relationship between hardness and indentation depth, as obtained by the indentation test. The strain hardening exponent n can also be obtained by Equation (18) [30]:

$$n=\frac{ln\sigma_{0.29}-ln\sigma_y}{ln150}\approx\frac{ln\sigma_{0.29}-ln\sigma_y}{5} \quad (18)$$

Finally, in this study, the plastic stress–strain constitutive model of the sintered nano-copper particles at room temperature is given by:

$$\sigma=\begin{cases}109.8\varepsilon\ (\sigma\leqslant 0.363\ GPa)\\ 0.363(1+302.47\varepsilon_p)^{0.399}\ (\sigma>0.363\ GPa)\end{cases} \quad (19)$$

High-temperature nanoindentation test result analysis

The temperature effect on indentation hardness

The indentation hardness of sintered nano-copper particles tested under different experimental temperatures is shown in Fig. 8, which indicates that the hardness values of tests samples prepared under three assisted pressures gradually decreased as the experimental temperature increased. The results revealed that the sintered nano-copper particles softened at higher temperatures, and its ability to resist plastic deformation decreased. Relevant study [31] indicated that the number of thermal vacancies exponentially increased as temperature increased, following the Arrhenius model as shown in Equation (20), which demonstrated that thermal vacancies generated at high temperatures could also increase the dislocation movement, resulting in a decrease in indentation hardness.

$$n_v=n\times exp\left(-\frac{Q_v}{RT_k}\right) \quad (20)$$

where, n_v is the number of vacancies, n is the number of atoms, Q_v is the active energy, R is the gas constant, and T_k is the Kelvin temperature.

In this study, the relationship between indentation hardness H and experimental temperature T of test samples was modeled following the exponential degradation law as described in Equation (21):

$$H=a\times Exp(K_HT)+b \quad (21)$$

where, H is indentation hardness in GPa, a and b are constants in the fitting equation, K_H is the degradation coefficient of hardness related to temperature, which is used to characterize the sensitivity of hardness to temperature, and it is also defined as the hardness temperature effect of sintered nano-copper particles. T is the temperature in Celsius.

According to Fig. 8, the indentation hardness of test samples under three assisted pressures were fitted with the experimental temperature through Equation (21), the results with fitting parameters are shown in Equations (22–24). As described in Equation (21), the greater the absolute value of the attenuation coefficient K_H, the more sensitive the material hardness is to temperature, and the faster the hardness decreases with an increase in temperature. On the one hand, the Berkovich diamond indenter used in this nanoindentation test was sharp, resulting in large deformation and local stress concentrations around the tip of the test sample, thus causing a large number of vacancies [27]. Vacancies can affect dislocation movement, resulting in decreased hardness with increasing temperature. On the other hand, at the same test temperature, the hardness increased with an increase in assisted pressure. Moreover, with the increase in assisted pressure, the absolute value of the hardness temperature effect factor decreased, indicating that the increase in assisted pressure can reduce the sensitivity of hardness to temperature. This can be explained that higher assisted pressure can significantly promote diffusion bonding between nano-copper particles, resulting in better bonding quality and sintering densification.

$H=12.248\times Exp(-\frac{T}{27.285})+0.594$, (10 MPa) (22)

$H=9.131\times Exp(-\frac{T}{35.275})+0.559$, (20 MPa) (23)

$H=19.045\times Exp(-\frac{T}{36.746})+0.615$, (30 MPa) (24)

The temperature effect of indentation modulus

Fig. 9 shows the indentation modulus of sintered nano-copper particles tested under different experimental temperatures, which presents that the indentation modulus decreased with an increase in temperature. This can be explained that the active atomic range expands and the distance between the atoms increases at higher temperatures, resulting in a soften of sintered nano-copper particles [32]. A linear degradation model between the indentation modulus and experimental temperature is proposed as shown in Equation (25):

$$E=A+K_E\times T \quad (25)$$

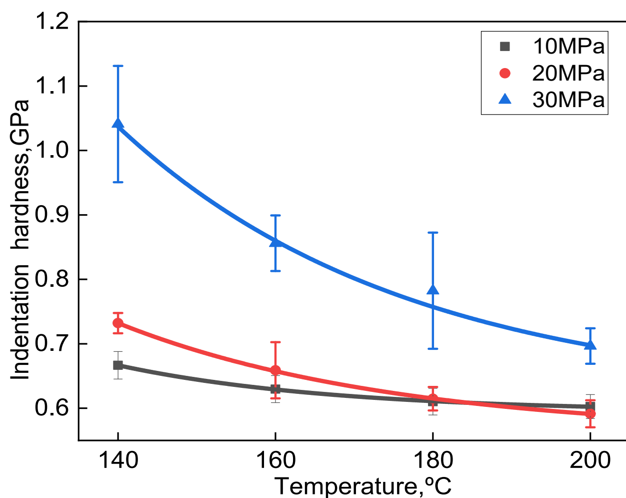

Fig. 8. The effect of temperature on the hardness of sintered nano-copper particles.

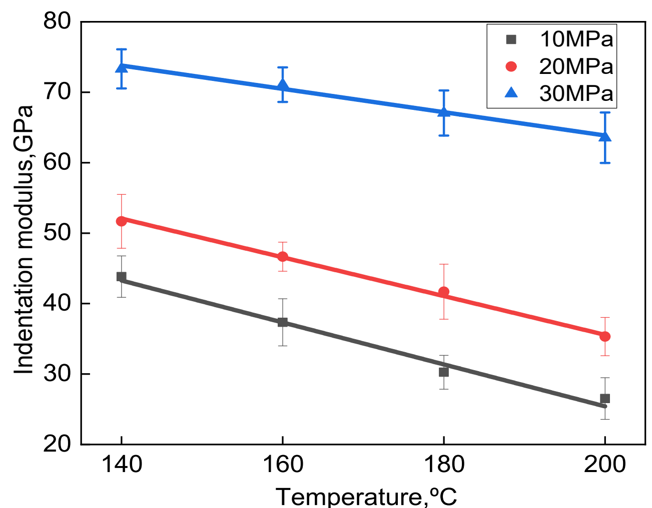

Fig. 9. The effect of temperature on the indentation modulus of sintered nano-copper particles.

where, E is indentation modulus in GPa, A is a constant, K_E is the degradation coefficient of the indentation modulus related to temperature, which is used to characterize the sensitivity of indentation modulus to temperature, and is defined as the temperature effect factor of indentation modulus. T is the temperature in Celsius.

The fitting results between indentation modulus and experimental temperature of test samples prepared under three assisted pressures are shown in Fig. 9, and the fitting models are list in Equations (26–28). The greater the absolute value of the temperature effect factor of indentation modulus K_E, the faster the decrease in indentation modulus. As the assisted pressure increases, the the temperature effect of indentation modulus decreases, indicating that the increase in assisted pressure reduces the sensitivity of the indentation modulus to temperature. Under the three sintering conditions, the absolute value of K_E was the largest at an assisted pressure of 10 MPa, indicating that the indentation modulus of test samples at this condition was the most sensitive to temperature.

$E = 80.27 - 0.29T$, (10 MPa) (26)

$E = 90.57 - 0.27T$, (20 MPa) (27)

$E = 96.95 - 0.16T$, (30 MPa) (28)

High temperature creep property analysis

Fig. 10 (a-c) show the indentation load–displacement relationship curves of sintered nano-copper particles prepared under three assisted pressures, those shows that the indentation curves of test samples moved to the right during the loading stage, and the indentation depth increased with an increase in experimental temperature from 140 to 200 ℃. Table 1 also quantitatively list the maximum indentation depths measured under an increase in experimental temperature, indicating that the sintered nano-copper particles gradually softened as the temperature increased. Besides, with an increase in assisted pressure, the indentation depth of test samples gradually decreased, and the sensitivity of indentation depth to temperature decreased, which reveals that the increasing assisted pressure can improve the elastic–plastic deformation resistance of sintered nano-copper particles.

Table 1
The maximum indentation depths at different temperatures and assisted pressures.

T/CP/MPa	140	160	180	200
10	1647 nm	1825 nm	2027 nm	2537 nm
20	1570 nm	1722 nm	1925 nm	2319 nm
30	1065 nm	1380 nm	1478 nm	1770 nm

Furthermore, as shown in Fig. 10, in the holding stage, the platform length of the indentation load–displacement curve increased gradually, and the creep depth increased as the experimental temperature increased. During creep test, the holding time at the peak load was maintained for 300 s, and then the data after 100 s were selected for analysis and calculating the steady-state creep performance of test samples. Fig. 11 (a-c) show the creep displacement–time curves of test samples treaded at different experimental temperatures. Table 2 lists the creep rates for the steady-state creep stage at different temperatures. As shows, the steady-state creep rate of test samples increased with an increase in experimental temperature. At high temperatures, the dislocation movement of sintered nano-copper particles intensified, their grain boundary strengths decreased, and the creep deformation resistance weakened. When the assisted pressure increased, the creep rate of samples tested at the same temperature decreased, indicating that their creep resistances were enhanced as the bonding strength of sintered nano-copper particles were further improved.

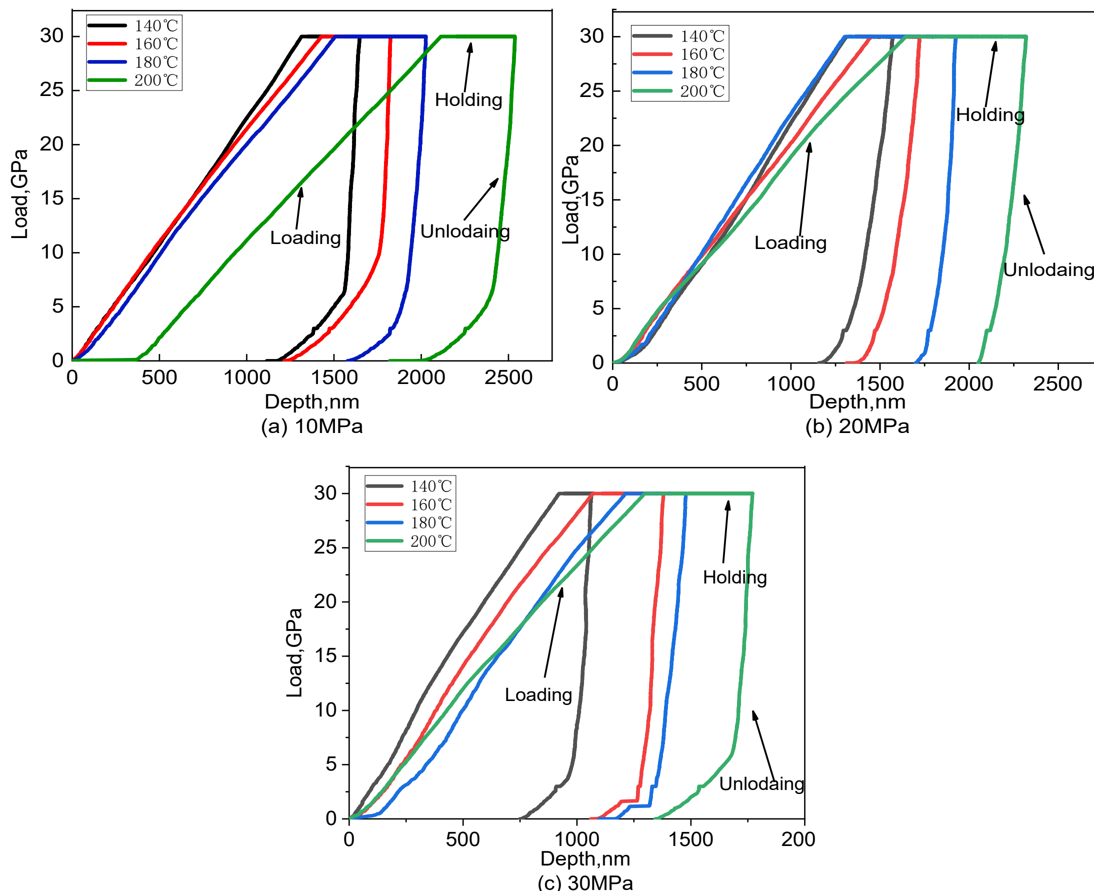

Fig. 10. The effect of temperature on the indentation load–displacement curves of test samples under three assisted pressures: (a) 10 MPa; (b) 20 MPa; (c) 30 MPa.

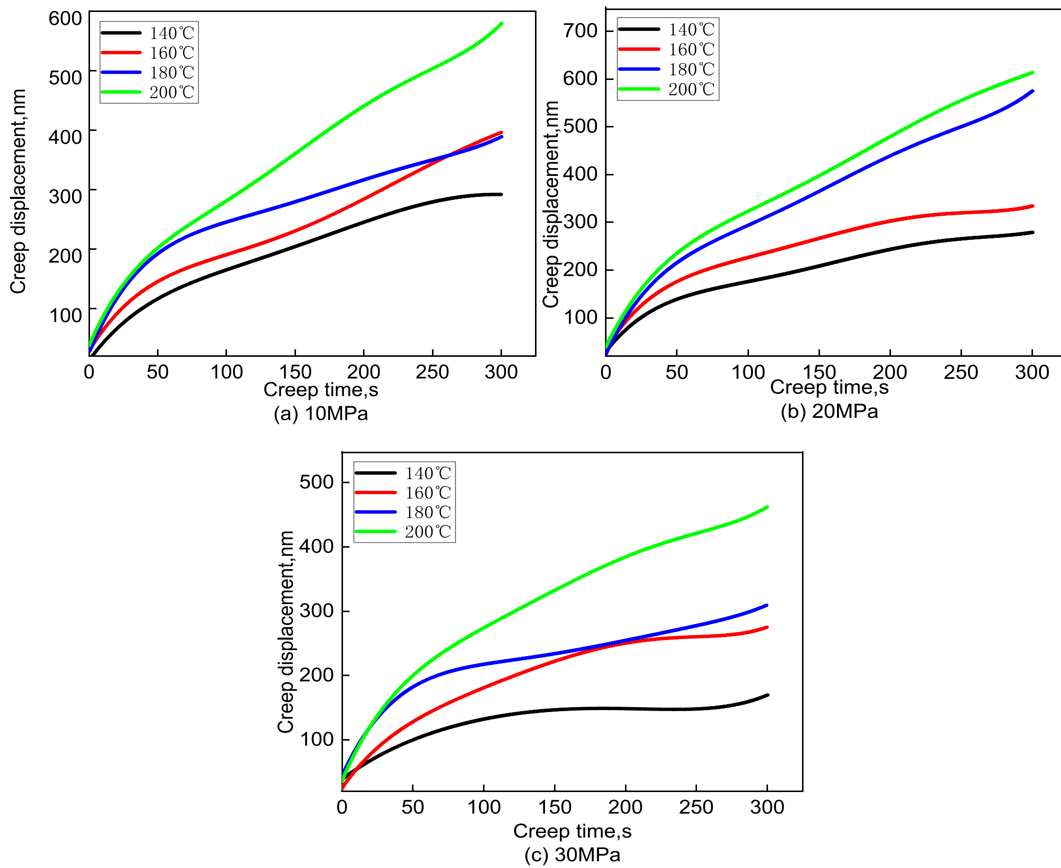

Fig. 11. The effect of temperature on creep of test samples under three assisted pressures: (a) 10 MPa; (b) 20 MPa; (c) 30 MPa.

Table 2
The steady-state creep rates at different temperatures and assisted pressures.

T/°CP/ MPa	140	160	180	200
10	2.85×10^{-3}. s^{-1}	4.21×10^{-3}. s^{-1}	6.44×10^{-3}. s^{-1}	7.43×10^{-3}. s^{-1}
20	1.91×10^{-3}. s^{-1}	2.02×10^{-3}. s^{-1}	2.86×10^{-3}. s^{-1}	3.46×10^{-3}. s^{-1}
30	1.31×10^{-3}. s^{-1}	1.86×10^{-3}. s^{-1}	2.37×10^{-3}. s^{-1}	2.56×10^{-3}. s^{-1}

Conclusion

In this study, the high temperature nanoindentation test was used to characterize the mechanical properties of sintered nano-copper particles used in high power electronics packaging. The results can be concluded as follows: (1) The hardness and indentation modulus of sintered nano-copper particles as prepared are depended on the loading rate and applied load. As the loading rate increased, their hardness and indentation modulus gradually increased and then kept stable. With an increase in applied load, their hardness and indentation modulus gradually decreased and then gradually stabilized. (2) The strain hardening index of sintered nano-copper particles was extracted from indentation load–displacement curves, and its room temperature constitutive model was then established. (3) The increase in assisted pressure, resulting in lower porosity and better bonding quality and sintering densification, made the hardness and indentation modulus of sintered nano-copper particles less sensitive to temperature. (4) The steady-state creep rate of sintered nano-copper particles increased as the operation temperature increased, and the creep deformation resistance decreased, however, their creep deformation resistance can be enhanced by increasing the assisted pressure.

CRediT authorship contribution statement

Jiajie Fan: Conceptualization, Methodology, Writing – review & editing, Project administration, Funding acquisition, Supervision. **Dawei Jiang:** Investigation, Data curation, Writing – original draft. **Hao Zhang:** Formal analysis, Validation. **Dong Hu:** Formal analysis, Validation. **Xu Liu:** Formal analysis, Validation. **Xuejun Fan:** Supervision. **Guoqi Zhang:** Supervision.

Declaration of Competing Interest

The authors declare that they have no known competing financial interests or personal relationships that could have appeared to influence the work reported in this paper.

Acknowledgements

This work was supported by National Natural Science Foundation of China (51805147), Shanghai Pujiang Program (2021PJD002) and Taiyuan Science and Technology Development Funds (Jie Bang Gua Shuai Program).

References

[1] Shapiro AA, Bonner JK, Ogunseitan OA, Saphores J-D-M, Schoenung JM. Implications of Pb-free microelectronics assembly in aerospace applications. IEEE Trans Compon Packag Technol 2006;29(1):60–70.
[2] Fan JJ, Xu D, Zhang H, Qian C, Fan XJ, Zhang GQ. Experimental Investigation on the Sintering Kinetics of Nanosilver Particles Used in High-Power Electronic Packaging. IEEE Trans Compon Packag Manuf Technol 2020;10(7):1101–9.

[3] Schnabl K, Wentlent L, Mootoo K, Khasawneh S, Zinn AA, Beddow J, et al. Nanocopper Based Solder-Free Electronic Assembly. J Electron Mater 2014;43(12):4515–21.
[4] Kamyshny A, Magdassi S. Conductive Nanomaterials for Printed Electronics. Small 2015;10(17):3515–35.
[5] Ishizaki T, Usui M, Yamada Y. Thermal cycle reliability of Cu-nanoparticle joint. Microelectron Reliab 2015;55(9–10):1861–6.
[6] Zhang BY, Damian A, Zijl J, van Zeijl H, Zhang Y, Fan JJ, et al. In-air sintering of copper nanoparticle paste with pressure-assistance for die attachment in high power electronics. Journal of Materials Science-Materials in Electronics 2021;32(4):4544–55.
[7] Hu D, Cui Z, Fan JJ, Fan XJ, Zhang GQ. Thermal kinetic and mechanical behaviors of pressure-assisted Cu nanoparticles sintering: A molecular dynamics study. Results Phys 2020;19:103486.
[8] Li H, Jing H, Han Y, Lu G-Q, Xu L, Liu T. Interface evolution analysis of graded thermoelectric materials joined by low temperature sintering of nano-silver paste. J Alloy Compd 2016;659:95–100.
[9] H. Zeijl Y. Carisey A. D. amian, R. H. Poelma, A. Zinn, and C. Q. Zhang, Metallic Nanoparticle Based Interconnect for Heterogeneous 3D Integration 2016 IEEE 66th Electronic Components and Technology Conference (ECTC) 2016 217 224.
[10] Liu X, Nishikawa H. Low-pressure Cu-Cu bonding using in-situ surface-modified microscale Cu particles for power device packaging. Scr Mater 2016;120:80–4.
[11] Liu JD, Chen HT, Ji HJ, Li MY. Highly Conductive Cu-Cu Joint Formation by Low-Temperature Sintering of Formic Acid-Treated Cu Nanoparticles. ACS Appl. Mater. Interfaces 2016;8(48):33289–98.
[12] Li J, Yu X, Shi T, Cheng C, Fan J, Cheng S, et al. Low-Temperature and Low-Pressure Cu–Cu Bonding by Highly Sinterable Cu Nanoparticle Paste. Nanoscale Res Lett 2017;12(1). https://doi.org/10.1186/s11671-017-2037-5.
[13] Nishikawa H, Hirano T, Takemoto T, Terada N. Effects of Joining Conditions on Joint Strength of Cu/Cu Joint Using Cu Nanoparticle Paste. Open Surface Science Journal 2011;3(1):60–4.
[14] Yamakawa T, Takemoto T, Shimoda M, Nishikawa H, Terada N. Influence of Joining Conditions on Bonding Strength of Joints: Efficacy of Low-Temperature Bonding Using Cu Nanoparticle Paste. J Electron Mater 2013;42(6):1260–7.
[15] Zuo Y, Shen J, Xu H, Gao R. Effect of different sizes of Cu nanoparticles on the shear strength of Cu-Cu joints. Mater Lett 2017;199:13–6.
[16] Chen C, Nagao S, Suganuma K, Jiu J, Sugahara T, Zhang H, et al. "Macroscale and microscale fracture toughness of microporous sintered Ag for applications in power electronic devices."*Acta*. Materialia 2017;129:41–51.
[17] Gadaud P, Caccuri V, Bertheau D, Carr J, Milhet X. Ageing sintered silver: Relationship between tensile behavior, mechanical properties and the nanoporous structure evolution. Mater Sci Eng, A 2016;669:379–86.
[18] Zabihzadeh S, Van Petegem S, Holler M, Diaz A, Duarte LI, Van Swygenhoven H. Deformation behavior of nanoporous polycrystalline silver. Part I: Microstructure and mechanical properties. Acta Mater 2017;131:467–74.
[19] Zhang H, Liu Y, Wang L, Sun F, Fan X, Zhang G. Indentation hardness, plasticity and initial creep properties of nanosilver sintered joint. Results Phys 2019;12:712–7.
[20] Jiang DW, Fan JJ, Hu D, Fan XJ, Zhang GQ. Study on the Mechanism of Nano-copper Particles Sintering Interconnection based on a non-isodiametric double sphere stacking model and Monte Carlo simulation. Transactions of the China Welding Institution 2021;42(3):07–13.
[21] Gao F, Nishikawa H, Takemoto T, Qu J. Mechanical properties versus temperature relation of individual phases in Sn–3.0Ag–0.5Cu lead-free solder alloy. Microelectron Reliab 2009;49(3):296–302.
[22] Imran M, Hussain F, Rashid M, Ahmad SA. Dynamic characteristics of nanoindentation in Ni: A molecular dynamics simulation study. Chin Phys B 2012;21(11):116201. https://doi.org/10.1088/1674-1056/21/11/116201.
[23] *Metallic materials - Instrumented indentation test for hardness and materials parameters - Part 1: Test method (ISO 14577-1:2015)*, 2016.
[24] Hsieh TH, Huang YS, Shen MY. Mechanical properties and toughness of carbon aerogel/epoxy polymer composites. J Mater Sci 2015;50(8):3258–66.
[25] Fischer-Cripps AC. Nanoindentation Testing. New York: Springer; 2011.
[26] Luo J, Lin J. A study on the determination of plastic properties of metals by instrumented indentation using two sharp indenters. Int J Solids Struct 2007;44(18–19):5803–17.
[27] Oliver WC, Pharr GM. An improved technique for determining hardness and elastic modulus using load and displacement sensing indentation experiments. J Mater Res 1992;7(06):1564–83.
[28] Albrecht H-J, Hannach T, Häse A, Juritza A, Müller K, Müller WH. Nanoindentation: a suitable tool to determine local mechanical properties in microelectronic packages and materials? Arch Appl Mech 2005;74(11-12):728–38.
[29] Wang FJ, Qian YY, Ma X. Measurement of mechanical properties of Sn-Ag-Cu bulk solder BGA solder joint using nanoindentation. Acta Metallurgica Sinica -Chinese Edition- 2005;41(7):775–9.
[30] Giannakopoulos AE, Suresh S. Determination of elastoplastic properties by instrumented sharp indentation. Scr Mater 1999;40(10):1191–8.
[31] George EP, Baker I. Thermal vacancies and the yield anomaly of FeAl. Intermetallics 1998;6(7-8):759–63.
[32] Ma H, Suhling JC. A review of mechanical properties of lead-free solders for electronic packaging. J Mater Sci 2009;44(5):1141–58.